Article

Tunable Microwave Dielectric Properties of Ca$_{0.6}$La$_{0.8/3}$TiO$_3$ and Ca$_{0.8}$Sm$_{0.4/3}$TiO$_3$-Modified (Mg$_{0.6}$Zn$_{0.4}$)$_{0.95}$Ni$_{0.05}$TiO$_3$ Ceramics with a Near-Zero Temperature Coefficient

Chung-Long Pan [1], **Chun-Hsu Shen** [2], **Shih-Hung Lin** [2,*] and **Qi-Zi Lin** [2]

[1] Department of Electrical Engineering, I-Shou University, No. 1, Sec. 1, Syuecheng Rd., Dashu District, Kaohsiung City 84001, Taiwan; ptl@isu.edu.tw

[2] Department of Electronic Engineering, National Yunlin University of Science and Technology, Section 3, 123 University Road, Douliou, Yunlin 64002, Taiwan; jameschs@yuntech.edu.tw (C.-H.S.); M10913071@yuntech.edu.tw (Q.-Z.L.)

[*] Correspondence: isshokenmei@yuntech.edu.tw; Tel.: +886-5-5342601 (ext. 4344); Fax: +886-5-5312063

Abstract: The microstructures and microwave dielectric properties of (Mg$_{0.6}$Zn$_{0.4}$)$_{0.95}$Ni$_{0.05}$TiO$_3$ with Ca$_{0.6}$La$_{0.8/3}$TiO$_3$ and Ca$_{0.8}$Sm$_{0.4/3}$TiO$_3$ additions prepared by the solid-state method has been investigated. The crystallization and microstructures of these two mixed dielectrics were checked by XRD, EDX, BEI, and SEM to demonstrate two phase systems. Furthermore, the tunable dielectric properties can be achieved by adjusting the amounts of Ca$_{0.6}$La$_{0.8/3}$TiO$_3$ and Ca$_{0.8}$Sm$_{0.4/3}$TiO$_3$ additions, respectively. After optimization of processed parameters, a new dielectric material system 0.88(Mg$_{0.6}$Zn$_{0.4}$)$_{0.95}$Ni$_{0.05}$TiO$_3$-0.12Ca$_{0.6}$La$_{0.8/3}$TiO$_3$ possesses a permittivity (ε_r) of 24.7, a Qf value of 106,000 (GHz), and a τ_f value of 3.8 (ppm/°C), with sintering temperature at 1225 °C for 4 h. This dielectric system with a near-zero temperature coefficient and appropriate microwave properties revealed a high potential for high-quality substrates adopted in wireless communication devices.

Keywords: temperature coefficient; dielectric properties; wireless communication; near-zero temperature coefficient

1. Introduction

With the ever-growing requirements of wireless communication devices and systems, there is a rapidly evolving lack of high-performance microwave circuits, receivers, transceivers, etc., to address the numerous 5G wireless communications technologies. Therefore, the utilization of dielectric ceramics with high permittivity (ε_r) and low dielectric loss has attracted more and more attention. In industrial applications, dielectric materials require the consideration of three parameters: an applicable relative permittivity (ε_r), a high-quality factor (Qf), and a near-zero temperature coefficient of resonance frequency (τ_f) [1–7]. Dielectric materials satisfied with these conditions demonstrated a reduction in component size and dielectric loss; conversely, the component characteristics are not affected by external temperature changes [8–10].

The MgTiO$_3$-based ceramics were documented as an ilmenite-type structure and showed an excellent dielectric performance in high-frequency applications [11]. To upgrade the dielectric performances of MgTiO$_3$-based ceramics, some studies focus on substituting Mg with M^{2+} (M^{2+} = Co, Ni, and Zn) and the (Mg$_{0.95}$M$^{2+}_{0.05}$)TiO$_3$ ceramics preserve the ilmenite-type structure [11,12]. Shen et al. [13] first reported Mg$_{0.95}$Ni$_{0.05}$TiO$_3$ with a Qf of 192,000 (GHz), ε_r ~17.35, and τ_f of –47 (ppm/°C) for the samples sintered at 1350 °C and 4 h. The main disadvantage of (Mg$_{0.95}$M$^{2+}_{0.05}$)TiO$_3$ ceramics is their high negative τ_f and, hence, difficulty to be practically utilized in microwave applications. Therefore, some researchers improved the microwave dielectric properties of (Mg$_{0.95}$M$^{2+}_{0.05}$)TiO$_3$ by mixing τ_f compensator [14]. With an appropriate stoichiometric of τ_f compensator additions, the mixture demonstrated near-zero τ_f with an appropriate

Qf value and permittivity. For example, it was found that the composition of $0.95MgTiO_3$-$0.05CaTiO_3$ ceramics has a zero τ_f. Furthermore, $Ca_{0.6}La_{0.8/3}TiO_3$ and $Ca_{0.8}Sm_{0.4/3}TiO_3$ were added in $Mg_{0.95}Ni_{0.05}TiO_3$ to obtain near-zero τ_f mixtures for practical applications in microwave components [15,16]. In addition, with the further substitution of Mg^{2+} (0.72 Å) by Zn^{2+}(0.82 Å), the $(Mg_{0.6}Zn_{0.4})_{0.95}Ni_{0.05}TiO_3$ ceramics were also synthesized by a traditional solid-state method that had been reported to possess *Qf* ~ 165,000 (GHz), ε_r of 19.3, and τ_f of −65.4 (ppm/°C) under sintering at 1200 °C/4 h by Lin et al. [17]. However, to our best knowledge, the microwave dielectric properties of $(Mg_{0.6}Zn_{0.4})_{0.95}Ni_{0.05}TiO_3$ with any τ_f compensator to adjust τ_f approaching zero have not been studied. The thermal budget of $(Mg_{0.6}Zn_{0.4})_{0.95}Ni_{0.05}TiO_3$ (1200 °C * 4 h) showed an obvious reduction compared to $Mg_{0.95}Ni_{0.05}TiO_3$ (1350 °C * 4 h). Therefore, the study of low thermal budget $(Mg_{0.6}Zn_{0.4})_{0.95}Ni_{0.05}TiO_3$-based ceramics with near-zero temperature coefficient and satisfied microwave dielectric properties via τ_f compensators additions is crucial for industrial applications.

In this work, two state-of-the-art τ_f compensators, $Ca_{0.6}La_{0.8/3}TiO_3$ (ε_r ~ 117.4, *Qf* ~ 13,375 GHz, and τ_f ~ 217.2 ppm/°C) and $Ca_{0.8}Sm_{0.4/3}TiO_3$ (ε_r ~ 120, *Qf* ~ 13,800 GHz, and τ_f ~ 400 ppm/°C), were chosen to mix with $(Mg_{0.6}Zn_{0.4})_{0.95}Ni_{0.05}TiO_3$ to characterize their dielectric properties, respectively. The mixtures of $x(Mg_{0.6}Zn_{0.4})_{0.95}Ni_{0.05}TiO_3$-(1 − x) $Ca_{0.6}La_{0.8/3}TiO_3$/$Ca_{0.8}Sm_{0.4/3}TiO_3$, which clarify the enhancement of its temperature coefficient characteristics for the achievement of a near-zero τ_f point. Densification, X-ray diffraction patterns, and microstructures were employed to analyze the physical properties of mixtures. The correlation between physical properties and microwave properties was investigated in detail and depth. Furthermore, the comparisons of thermal budget and microwave dielectric properties between $(Mg_{0.6}Zn_{0.4})_{0.95}Ni_{0.05}TiO_3$ (1200 °C * 4 h) and $Mg_{0.95}Ni_{0.05}TiO_3$ (1350 °C * 4 h) with τ_f compensators were presented.

2. Results and Discussion

2.1. Physical Investigation

The XRD analysis for $x(Mg_{0.6}Zn_{0.4})_{0.95}Ni_{0.05}TiO_3$-(1–x)$Ca_{0.6}La_{0.8/3}TiO_3$/$Ca_{0.8}Sm_{0.4/3}TiO_3$ (hereafter referred to as xMZNT-(1–x)CLa/CSm) with x = 0.88 sintered at 1175 °C–1300 °C for 4 h and sintered at 1225 °C ($Ca_{0.6}La_{0.8/3}TiO_3$)/1250 °C ($Ca_{0.8}Sm_{0.4/3}TiO_3$) for 4 h with various x values, are illustrated in Figure 1a,b, respectively. The X-ray patterns indicated the presence of $(Mg_{0.6}Zn_{0.4})_{0.95}Ni_{0.05}TiO_3$ signals as the primary crystalline phase with a less minor phase of $Ca_{0.6}La_{0.8/3}TiO_3$ (ICDD-PDF #22-0153) or $Ca_{0.8}Sm_{0.4/3}TiO_3$(ICDD-PDF #78-1371) [18,19], and the second phase of $(Mg_{0.6}Zn_{0.4})_{0.95}Ni_{0.05}Ti_2O_5$ (which can be referred to as $MgTi_2O_5$). It was reported that the crystal structures of $(Mg_{0.6}Zn_{0.4})_{0.95}Ni_{0.05}TiO_3$ are hexagonal, and those of $Ca_{0.6}La_{0.8/3}TiO_3$ and $Ca_{0.8}Sm_{0.4/3}TiO_3$ are cubic. $(Mg_{0.6}Zn_{0.4})_{0.95}Ni_{0.05}Ti_2O_5$ with the orthorhombic crystal structure (ICDD-PDF #00009–0016), usually formed as an intermediate phase, was identified and difficult to remove from the $MgTiO_3$-based sample composed by the traditional mixed oxide route [20–22]. The composition of the second phase $(Mg_{0.6}Zn_{0.4})_{0.95}Ni_{0.05}Ti_2O_5$, which might diminish the *Qf* values of the specimen [22], has primarily resulted from the loss of ignition (LOI) of the raw powder MgO. The following reaction (Equation (1)) may explain this phenomenon:
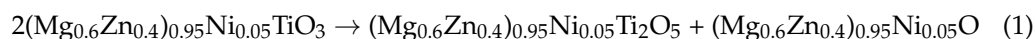
$$2(Mg_{0.6}Zn_{0.4})_{0.95}Ni_{0.05}TiO_3 \rightarrow (Mg_{0.6}Zn_{0.4})_{0.95}Ni_{0.05}Ti_2O_5 + (Mg_{0.6}Zn_{0.4})_{0.95}Ni_{0.05}O \quad (1)$$

$\ast: (Mg_{0.6}Zn_{0.4})_{0.95}Ni_{0.05}TiO_3 、 \mathbf{O}: Ca_{0.8}Sm_{0.4/3}TiO_3 、 \triangle: Ca_{0.6}La_{0.8/3}TiO_3 、 +: (Mg_{0.6}Zn_{0.4})_{0.95}Ni_{0.05}Ti_2O_5$

(a)

$\ast: (Mg_{0.6}Zn_{0.4})_{0.95}Ni_{0.05}TiO_3 、 \mathbf{O}: Ca_{0.8}Sm_{0.4/3}TiO_3 、 \triangle: Ca_{0.6}La_{0.8/3}TiO_3 、 +: (Mg_{0.6}Zn_{0.4})_{0.95}Ni_{0.05}Ti_2O_5$

(b)
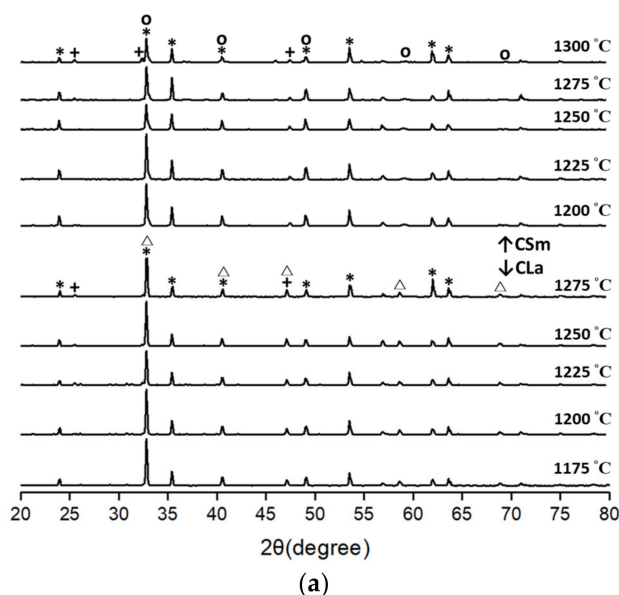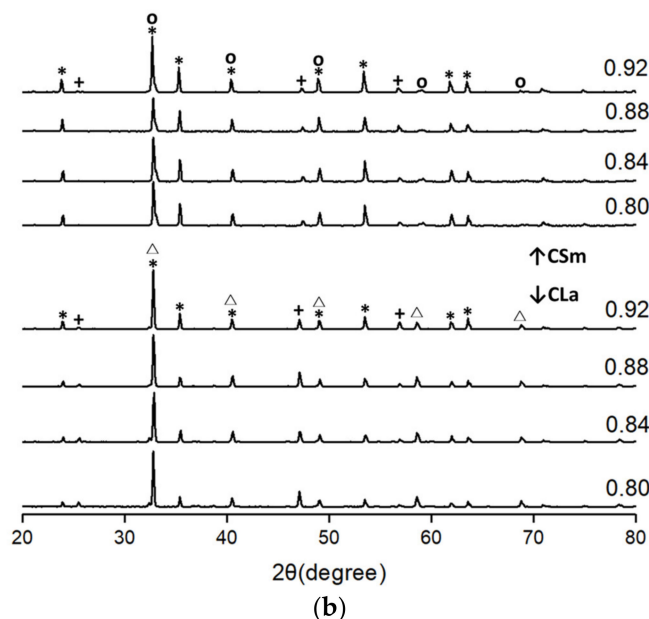
Figure 1. X-ray diffraction illustrations of (**a**) $0.88(Mg_{0.6}Zn_{0.4})_{0.95}Ni_{0.05}TiO_3$-$0.12$ $Ca_{0.6}La_{0.8/3}TiO_3/Ca_{0.8}Sm_{0.4/3}TiO_3$ ceramics sintered at various temperatures for 4 h, (**b**) $x(Mg_{0.6}Zn_{0.4})_{0.95}Ni_{0.05}TiO_3$-$(1 - x)Ca_{0.6}La_{0.8/3}TiO_3$ sintered at 1225 °C for 4 h /$Ca_{0.8}Sm_{0.4/3}TiO_3$ sintered at 1250 °C for 4 h with various x values.

X-ray diffraction results of the xMZNT-$(1 - x)$CLa/CSm systems demonstrated no significant change with varying sintering temperature and x value.

The lattice parameters of $(Mg_{0.6}Zn_{0.4})_{0.95}Ni_{0.05}TiO_3$ mixed phase ceramics as a function of sintering temperature and x value were also calculated, as shown in Figure 2a,b. A minor increase in both a-site and c-site was found for $(Mg_{0.6}Zn_{0.4})_{0.95}Ni_{0.05}TiO_3$ ceramics with the confronting of $MgTiO_3$ (ICDD–PDF #00-006-0494). The consequences clarify that $(Mg_{0.6}Zn_{0.4})_{0.95}Ni_{0.05}TiO_3$ ceramics would compose a solid solution to replace Mg^{2+} with Zn^{2+}. The lattice parameters vary from a = 5.054 Å and c = 13.898 Å of $MgTiO_3$ [21] to a = 5.07 Å, and c = 13.923 Å with the formation of $(Mg_{0.6}Zn_{0.4})_{0.95}Ni_{0.05}TiO_3$[19]. The reason is that the ionic radii of Zn^{2+}(0.82 Å) are much bigger than those of Mg^{2+}

(0.72 Å). With the $Ca_{0.8}Sm_{0.4/3}TiO_3$ and $Ca_{0.6}La_{0.8/3}TiO_3$ additions, the lattice parameters of xMZNT-(1 − x)CLa/CSm ceramics don't vary significantly with the increasing amounts of $Ca_{0.6}La_{0.8/3}TiO_3$ and $Ca_{0.8}Sm_{0.4/3}TiO_3$. This explanation proved the existence of a two phase system of xMZNT-(1 − x)CLa/CSm ceramics and strongly agreed with XRD patterns results shown in Figure 1.
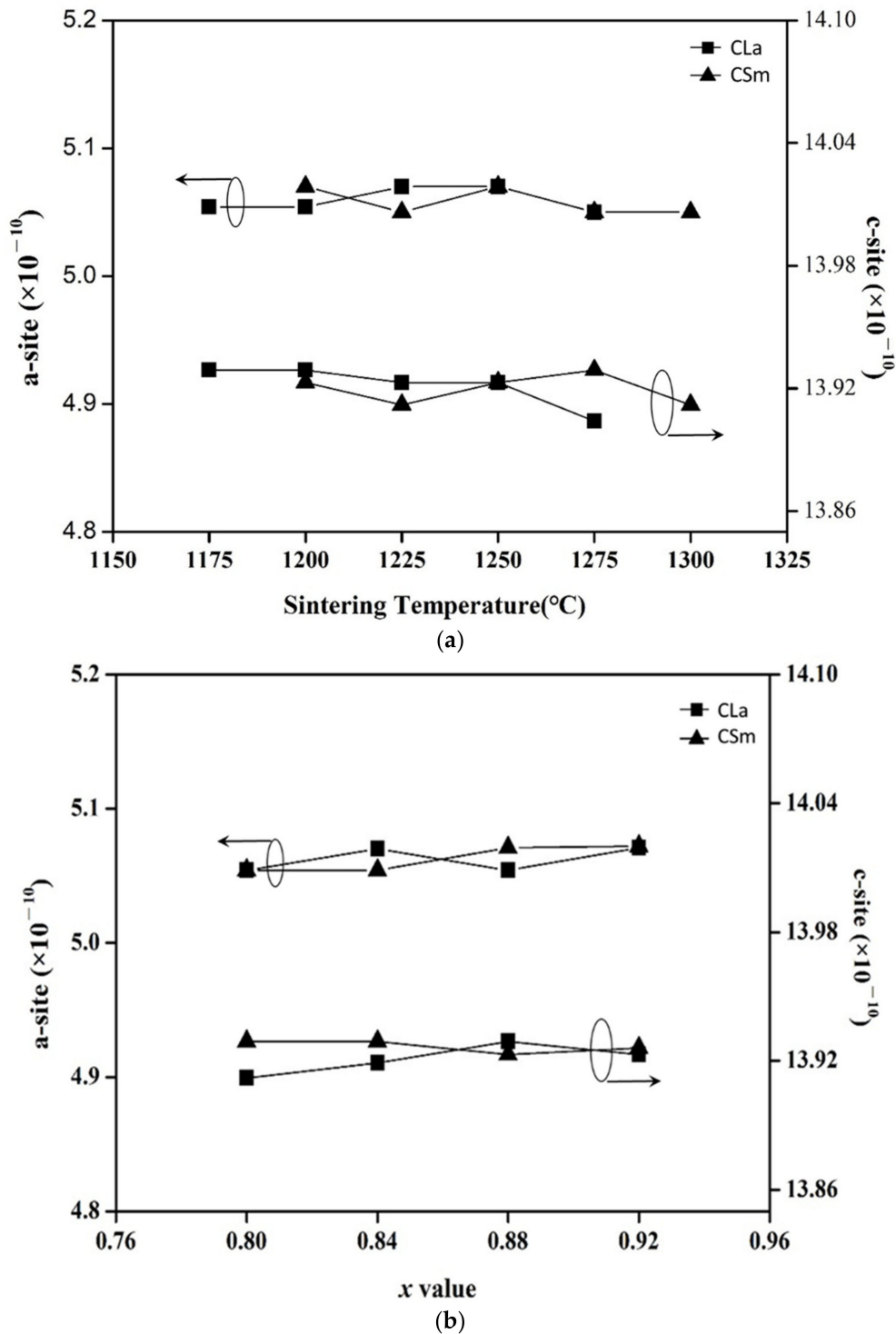
Figure 2. Lattice parameters of (**a**) $0.88(Mg_{0.6}Zn_{0.4})_{0.95}Ni_{0.05}TiO_3$-$0.12Ca_{0.6}La_{0.8/3}TiO_3/Ca_{0.8}Sm_{0.4/3}TiO_3$ at various sintering temperature, (**b**) $x(Mg_{0.6}Zn_{0.4})_{0.95}Ni_{0.05}TiO_3$-(1 − x) $Ca_{0.6}La_{0.8/3}TiO_3$ sintered at 1225 °C and $Ca_{0.8}Sm_{0.4/3}TiO_3$ sintered at 1250 °C.

The microstructure photographs of xMZNT-(1 − x)CLa/CSm ceramics under x = 0.88 with different sintering temperatures and sintered at 1225 °C ($Ca_{0.6}La_{0.8/3}TiO_3$)/1250 °C ($Ca_{0.8}Sm_{0.4/3}TiO_3$) with varying values of x were revealed in Figures 3 and 4, respectively. The average size of grains increased with the increasing sintering temperature, and microstructures revealed the most compact and the fewest pores at 1225 °C ($Ca_{0.6}La_{0.8/3}TiO_3$)/1250 °C ($Ca_{0.8}Sm_{0.4/3}TiO_3$). Moreover, the grain growth rate of $(Mg_{0.6}Zn_{0.4})_{0.95}Ni_{0.05}TiO_3$ was much more rapid than that of $Ca_{0.8}Sm_{0.4/3}TiO_3$ or $Ca_{0.6}La_{0.8/3}TiO_3$, which would result in a great size disparity in the specimens. This phenomenon exhibits that the existence of a $Ca_{0.8}Sm_{0.4/3}TiO_3$ or $Ca_{0.6}La_{0.8/3}TiO_3$ phase may repress irregular grain growth of the main phases, which supports the attainment of an excellent dielectric performance. However, excess amounts of $Ca_{0.6}La_{0.8/3}TiO_3$/$Ca_{0.8}Sm_{0.4/3}TiO_3$ contributed to the dielectric loss of the ceramics system, and high porosity may have directly affected the dielectric performances of the ceramic specimens. Furthermore, we also studied the specimens' microstructures with x = 0.80–0.92 at the optimal sintering temperature for xMZNT-(1 − x)CLa/CSm under 1225 °C ($Ca_{0.6}La_{0.8/3}TiO_3$)/1250 °C ($Ca_{0.8}Sm_{0.4/3}TiO_3$). Generally speaking, well-densified samples with tiny porosity were obtained when samples sintered at 1225 °C ($Ca_{0.6}La_{0.8/3}TiO_3$)/1250 °C ($Ca_{0.8}Sm_{0.4/3}TiO_3$) with x = 0.80–0.92, but the surface morphology of the xMZNT-(1 − x)CLa/CSm varied significantly under x = 0.88 with a different sintering temperature.

(**a**) x = 0.88 at 1175 °C   (**b**) x = 0.88 at 1200 °C   (**c**) x = 0.88 at 1225 °C

(**d**) x = 0.88 at 1250 °C   (**e**) x = 0.88 at 1275 °C   (**f**) x = 0.8 at 1225 °C

(**g**) x = 0.84 at 1225 °C   (**h**) x = 0.92 at 1225 °C
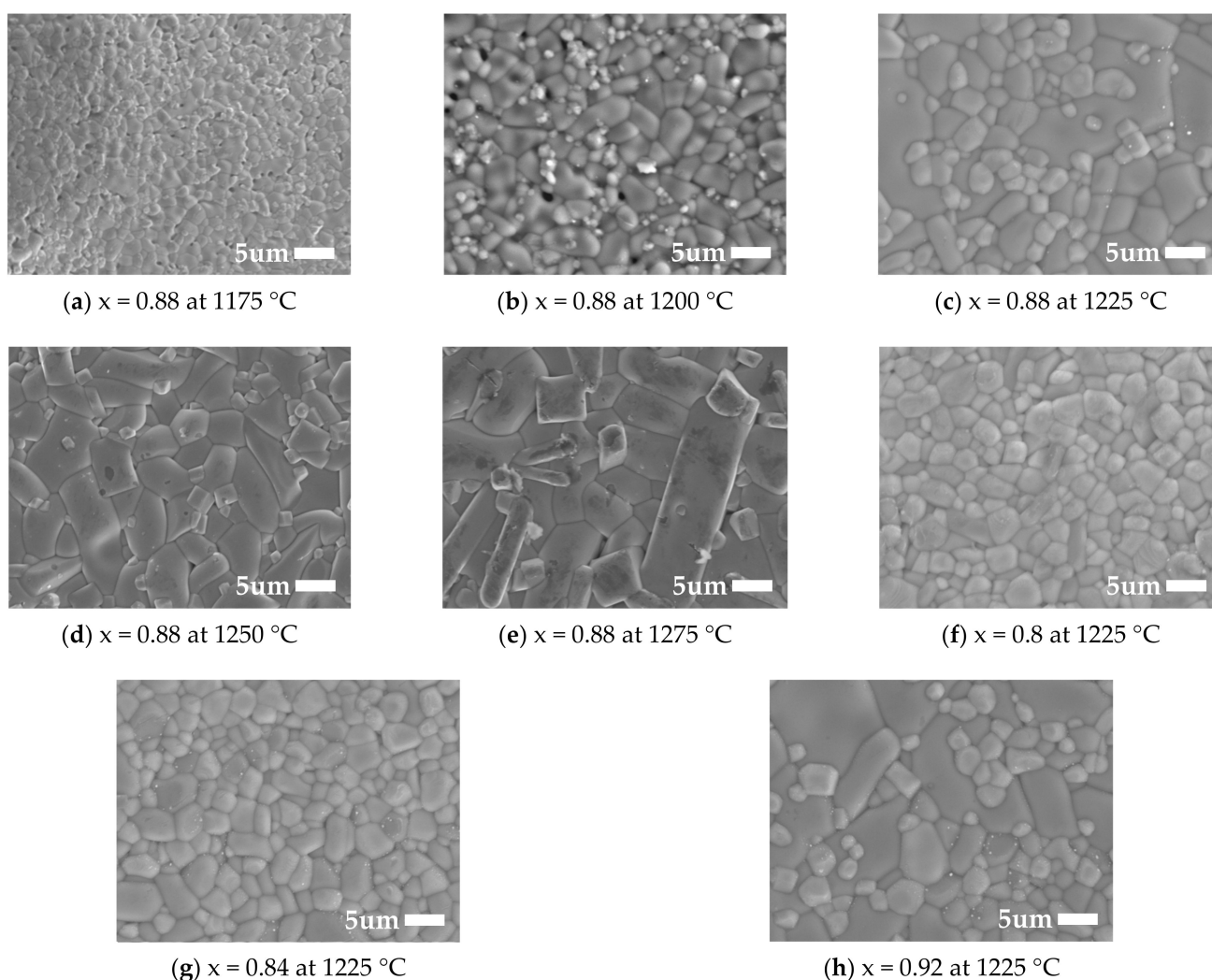
Figure 3. (**a**–**h**) Scanning electron microscopy photographs of $Ca_{0.6}La_{0.8/3}TiO_3$-modified $(Mg_{0.6}Zn_{0.4})_{0.95}Ni_{0.05}TiO_3$ with x = 0.88 sintered from 1175 °C to 1275 °C for 4 h and with various x values sintered at 1225 °C for 4 h.

(**a**) x = 0.88 at 1200 °C   (**b**) x = 0.88 at 1225 °C   (**c**) x = 0.88 at 1250 °C

(**d**) x = 088 at 1275 °C   (**e**) x = 0.88 at 1300 °C   (**f**) x = 0.8 at 1250 °C

(**g**) x = 0.84 at 1250 °C   (**h**) x = 0.92 at 1250 °C
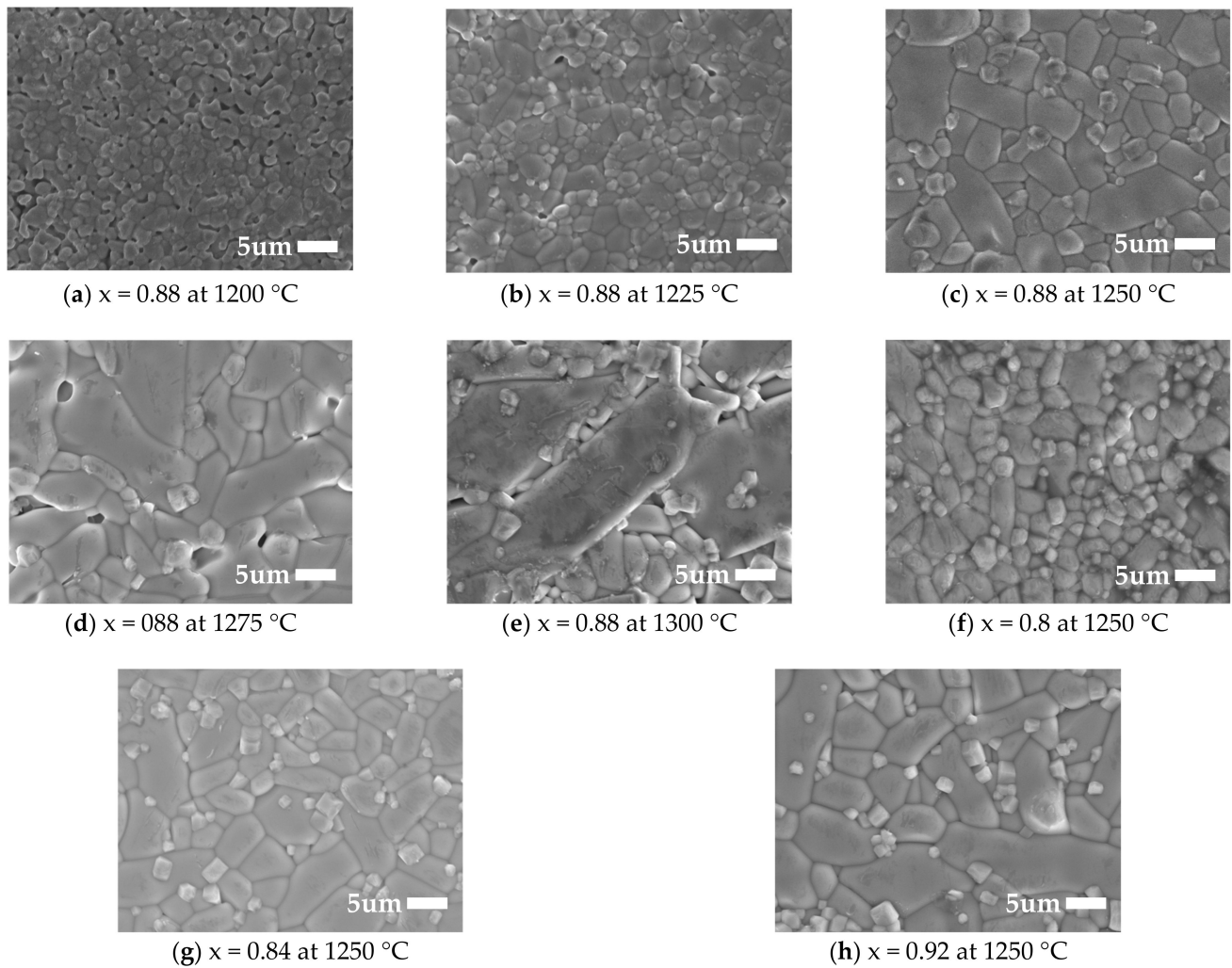
Figure 4. (**a–h**) Scanning electron microscopy photographs of $Ca_{0.8}Sm_{0.4/3}TiO_3$-modified $(Mg_{0.6}Zn_{0.4})_{0.95}Ni_{0.05}TiO_3$ with x = 0.88 sintered from 1200 °C to 1300 °C for 4 h and with various x values sintered at 1250 °C for 4 h.

Individual grain composition and distribution in the 0.88MZNT-0.12CLa/CSm ceramics sintered at 1225 °C ($Ca_{0.6}La_{0.8/3}TiO_3$)/1250 °C ($Ca_{0.8}Sm_{0.4/3}TiO_3$) were checked by EDS and the backscattered electronic image (BEI) as shown in Figure 5. The grains marked with spots A–J can be divided into three groups: huge dark grey polygons (spots A and C, and spots F and G), small bright grey polygons (spots D and E, and spots I and J), and small dark grey stick (spot B, and H). Huge polygons were distinguished as $(Mg_{0.6}Zn_{0.4})_{0.95}Ni_{0.05}TiO_3$ accompanying small polygons $Ca_{0.8}Sm_{0.4/3}TiO_3$ or $Ca_{0.6}La_{0.8/3}TiO_3$ crystallites nearby. The distributed small stick was indexed as $(Mg_{0.6}Zn_{0.4})_{0.95}Ni_{0.05}Ti_2O_5$, which is not a dominant element in the specimen. As expected, xMZNT-(1 − x)CLa/CSm phases separated since they exhibited virtually no solubility between them due to different crystal structures. This discussion was further confirmed in BEI analysis.

(a)   (b)
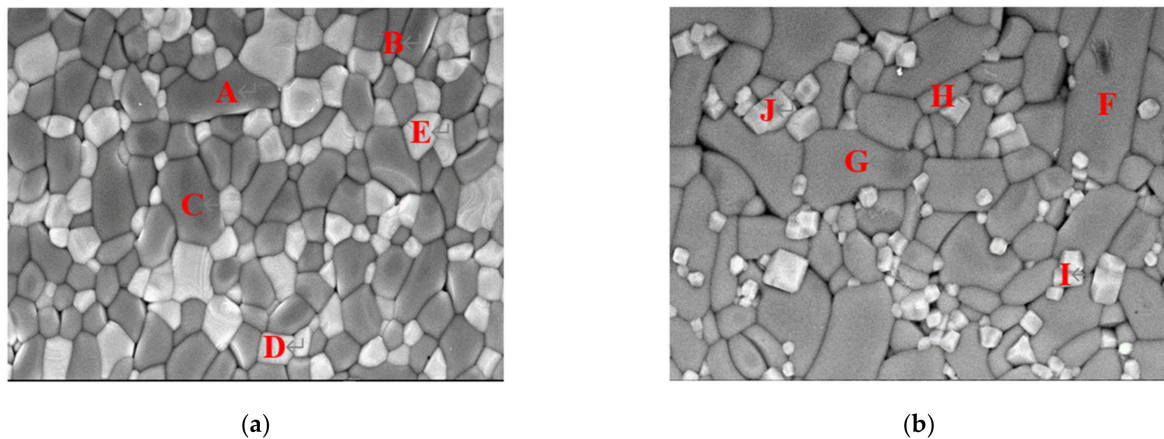
Spot	Atom (%)							
	MgK	**NiK**	**TiK**	**OK**	**ZnL**	**CaK**	**LaK**	**SmK**
A	9.4	0.32	9.92	73.42	6.94	0	0	0
B	11.94	1.18	21.53	57.33	8.02	0	0	0
C	7.89	0.27	10.67	85.21	5.96	0	0	0
D	0	0	10.54	85.95	0	2.25	1.26	0
E	0	0	10.43	84.75	0	3.27	1.55	0
F	14.64	0.82	14.45	62.79	7.3	0	0	0
G	12.55	0.76	14.3	65.05	7.33	0	0	0
H	10.93	0.94	19.62	61.55	6.97	0	0	0
I	0	0	25.02	50.65	0	20.79	0	3.54
J	0	0	29.57	44.11	0	22.9	0	3.43

Figure 5. The BEI photograph and EDS results of $(Mg_{0.6}Zn_{0.4})_{0.95}Ni_{0.05}TiO_3$ ceramics with (**a**) $Ca_{0.6}La_{0.8/3}TiO_3$ sintered at 1225 °C for 4 h, (**b**) $Ca_{0.8}Sm_{0.4/3}TiO_3$ additions sintered at 1250 °C for 4 h.

Figure 6 shows the apparent densities of the xMZNT-(1 − x)CLa/CSm ceramics system sintered at various temperatures for 4 h. With the rise in sintering temperature, the apparent density reached a maximum value of 1225 °C $(Ca_{0.6}La_{0.8/3}TiO_3)$/1250 °C $(Ca_{0.8}Sm_{0.4/3}TiO_3)$. This resulted from the ceramics' microstructure being denser, as observed in Figures 3 and 4. In addition, the apparent densities were also a function of the combinations and raised with the reducing x value due to the heavier nature of $Ca_{0.8}Sm_{0.4/3}TiO_3/Ca_{0.6}La_{0.8/3}TiO_3$ than $(Mg_{0.6}Zn_{0.4})_{0.95}Ni_{0.05}TiO_3$, as shown in Table 1.

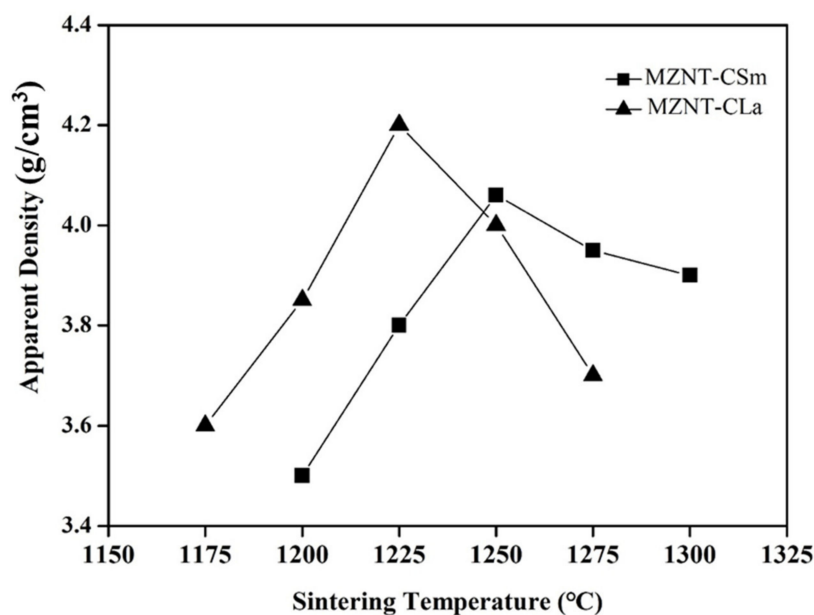**Figure 6.** Dependence of apparent density on sintering temperature of the $0.88(Mg_{0.6}Zn_{0.4})_{0.95}Ni_{0.05}TiO_3$-$0.12Ca_{0.6}La_{0.8/3}TiO_3/Ca_{0.8}Sm_{0.4/3}TiO_3$ ceramics.

Table 1. Microwave dielectric properties of $(Mg_{0.6}Zn_{0.4})_{0.95}Ni_{0.05}TiO_3$ with $Ca_{0.6}La_{0.8/3}TiO_3$ sintered at 1225 °C, and $Ca_{0.8}Sm_{0.4/3}TiO_3$ sintered at 1250 °C for 4 h.

$x(Mg_{0.6}Zn_{0.4})_{0.95}Ni_{0.05}TiO_3$-$(1 - x)Ca_{0.6}La_{0.8/3}TiO_3$					
x value	S.T.(°C)	Density (g/cm³)	ε_r	Qf (Hz)	τ_f (ppm/°C)
0.92		4.0	23.1	116,000	−44.0
0.88	1225	4.2	24.7	106,000	3.8
0.84		4.4	28.8	62,000	12.3
0.80		4.5	29.6	36,000	39.4
$x(Mg_{0.6}Zn_{0.4})_{0.95}Ni_{0.05}TiO_3$-$(1 - x)Ca_{0.8}Sm_{0.4/3}TiO_3$					
x value	S.T.(°C)	Density (g/cm³)	ε_r	Qf (Hz)	τ_f(ppm/°C)
0.92		4.05	21.8	92,000	−11.3
0.88	1250	4.06	23.8	72,000	4.3
0.84		4.10	26.1	60,000	30.9
0.80		4.40	28.1	40,000	91.2

S.T.: Sintering Temperature.

2.2. Microwave Dielectric Properties

The tunable dielectric properties of the xMZNT-(1 − x)CLa/CSm ceramics as a function of the sintering temperature and x value were shown in Figures 7 and 8, respectively. The correlation between permittivity (ε_r) and sintering temperatures exhibited an equivalent tendency between densities and sintering temperatures, because higher density is physically equivalent to lower porosity. The permittivity slightly increased with the rising sintering temperature. The ε_r of the $0.88(Mg_{0.6}Zn_{0.4})_{0.95}Ni_{0.05}TiO_3$-$0.12Ca_{0.6}La_{0.8/3}TiO_3$ ceramics gradually vary from 19.3 to 23.8 as the sintering temperature ranged from 1175 °C to 1225 °C and, after that, decreased after 1250 °C. Furthermore, the dielectric performances of the xMZNT-(1 − x)CLa/CSm ceramics as a function of the x value were shown in Figure 8. The ε_r was raised with a reducing x value due to a higher permittivity (ε_r) of $Ca_{0.6}La_{0.8/3}TiO_3$ and $Ca_{0.8}Sm_{0.4/3}TiO_3$ additions.
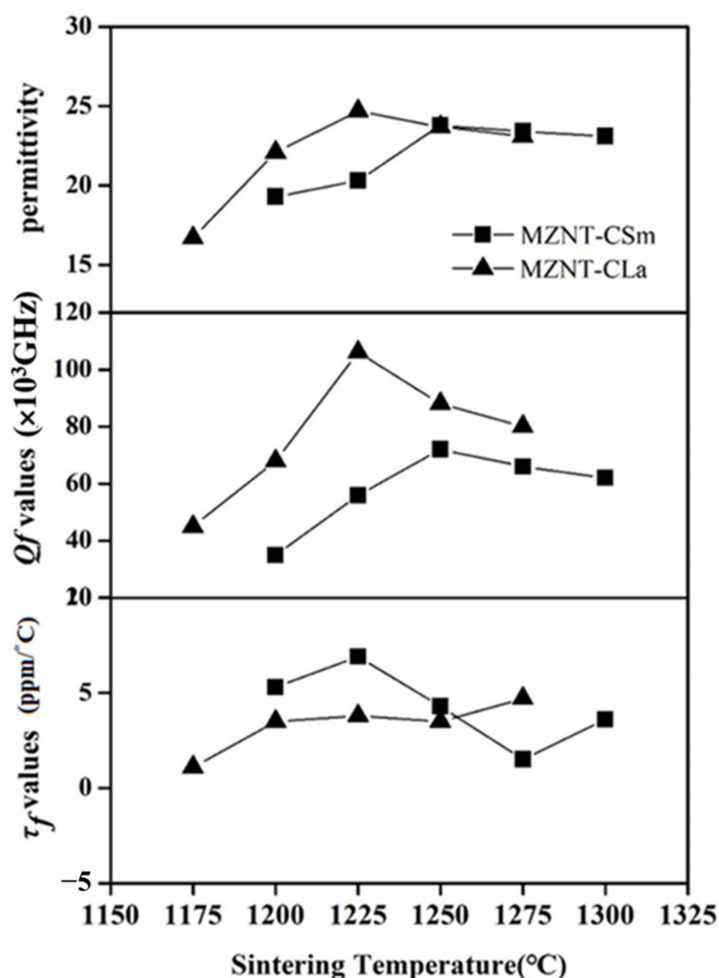
Figure 7. The dielectric properties of the $0.88(Mg_{0.6}Zn_{0.4})_{0.95}Ni_{0.05}TiO_3$-$0.12Ca_{0.6}La_{0.8/3}TiO_3$/$Ca_{0.8}Sm_{0.4/3}TiO_3$ ceramics as a function of the sintering temperature.

The quality factor is a significant symbol for the utilizations of dielectric ceramics at microwave frequency, since a higher quality factor means a lower dielectric loss for microwave frequency devices. The quality factor of $(Mg_{0.6}Zn_{0.4})_{0.95}Ni_{0.05}TiO_3$ is much higher than that of $Ca_{0.8}Sm_{0.4/3}TiO_3$ and $Ca_{0.6}La_{0.8/3}TiO_3$. Hence, it is supposed that the *Qf* values should reduce with the rising amount of $Ca_{0.6}La_{0.8/3}TiO_3$/$Ca_{0.8}Sm_{0.4/3}TiO_3$. The *Qf* values of xMZNT-(1 − x)CLa/CSm ceramics system reduce with the combination (x), as shown in Figure 8. The microwave dielectric loss is principally occasioned by the lattice vibrational modes, pores, and second phases [23]. The *Qf* value of xMZNT-(1 − x) CLa raised with the sintering temperature increased from 1175 °C to 1225 °C (maximum *Qf* at 1225 °C) and decreased gradually. The increment of *Qf* value at 1175 °C to 1225 °C was high relative to the density rise and the uniformity of grain growth, as observed in Figures 3 and 4. At 1225 °C, the maximum *Qf* value of around 106,000 GHz was measured for the $0.88(Mg_{0.6}Zn_{0.4})_{0.95}Ni_{0.05}TiO_3$-$0.12$ $Ca_{0.6}La_{0.8/3}TiO_3$ ceramics. The downgrade in *Qf* value was attributed to inhomogeneous grain growth, and resulted in a reduction in density shown in Figures 3 and 4. Since the *Qf* value of xMZNT-(1 − x)CLa/CSm ceramics was consistent with the variation of density, it implied that the dielectric loss of xMZNT-(1 − x)CLa/CSm ceramics was primarily dominated by the bulk density [24,25].

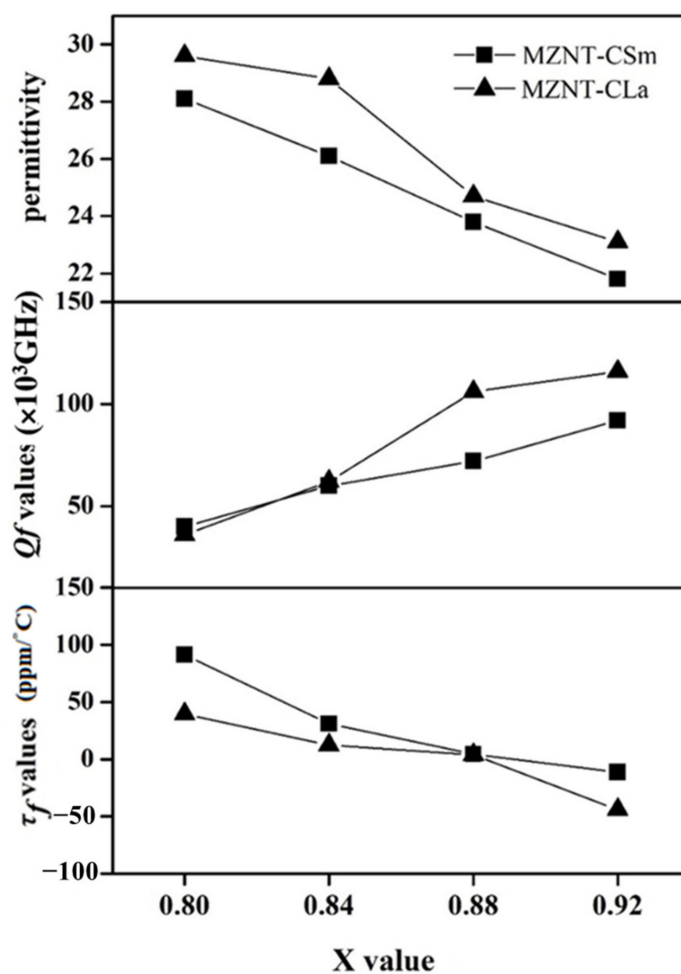**Figure 8.** The dielectric properties of the x$(Mg_{0.6}Zn_{0.4})_{0.95}Ni_{0.05}TiO_3$-$(1 − x)Ca_{0.6}La_{0.8/3}TiO_3$ sintered at 1225 °C/$Ca_{0.8}Sm_{0.4/3}TiO_3$ sintered at 1250 °C as a function of the x values.

The resonant frequency temperature coefficient is strongly related to the mixture, the additions, and the second phase of a material [26]. For example, the τ_f values of xMZNT-(1 − x)CLa/CSm ceramics rapidly improved with reducing x value due to τ_f compensator $Ca_{0.6}La_{0.8/3}TiO_3$/$Ca_{0.8}Sm_{0.4/3}TiO_3$ additions. However, a significant change in the τ_f value was not observed of specimens at different sintering temperatures; it only slightly varied from 1 to 7 ppm/°C as the temperature range remained below 100 °C. It also demonstrated a transition of τ_f value from negative to positive as x varied from 0.92 to 0.80. Thus, a near-zero τ_f value can be achieved by proper stoichiometric calculation.

Table 1 demonstrated the tunable microwave dielectric properties of xMZNT-(1 − x)CLa/CSm ceramic system. As the x value decreased from 0.92 to 0.80, the τ_f values of xMZNT-(1 − x)CLa ceramics at 1225 °C ranged from −44.0 to +39.4 ppm/°C, and xMZNT-(1 − x)CSm ceramics at 1250 °C ranged from −11.3 to +91.2 ppm/°C. The more comprehensive τ_f range for xMZNT-(1 − x)CSm mixture was due to the high value τ_f compensator addition of $Ca_{0.8}Sm_{0.4/3}TiO_3$ (~400 ppm/°C). We also consider Qf value at near-zero τ_f, and xMZNT-(1 − x)CLa revealed a higher Qf value. Overall, a ceramic system with the following properties: low sintering temperature, high Qf value, mostly near-zero τ_f values, etc., was regarded as a suitable dielectric mixture. Therefore, $0.88(Mg_{0.6}Zn_{0.4})_{0.95}Ni_{0.05}TiO_3$-$0.12\ Ca_{0.6}La_{0.8/3}TiO_3$ sintered at 1225 °C/4 h with a permittivity (ε_r) of 24.7, a Qf value of 106,000 GHz, and a τ_f value of 3.8 ppm/°C was recommended as the potential candidate adopted in practical applications.

Table 2 describes the microwave dielectric properties of relative dielectrics and mixtures with τ_f compensator. With $Ca_{0.6}La_{0.2667}TiO_3$ addition, $0.88(Mg_{0.6}Zn_{0.4})_{0.95}Ni_{0.05}TiO_3$-

0.12 $Ca_{0.6}La_{0.8/3}TiO_3$ demonstrated the 3.92% higher *Qf* and 8.2% lower thermal budget with comparable near-zero τ_f than $0.85Mg_{0.95}Ni_{0.05}TiO_3$-0.15 $Ca_{0.6}La_{0.8/3}TiO_3$. This improvement makes $(Mg_{0.6}Zn_{0.4})_{0.95}Ni_{0.05}TiO_3$-based ceramics a potential substrate material candidate for adoption in industrial applications. Surfing the applications of $0.88(Mg_{0.6}Zn_{0.4})_{0.95}Ni_{0.05}TiO_3$-0.12 $Ca_{0.6}La_{0.8/3}TiO_3$ in 5G wireless communications in the future is attractive.

Table 2. Comparison of the proposed dielectric with other similar reported dielectric ceramics.

Composition	S.T.(°C)	Permittivity	*Qf* (Hz)	τ_f (ppm/°C)	Ref
$(Mg_{0.95}Ni_{0.05})TiO_3$	1350 °C/4 h	17.35	192,000	−47.0	[13]
$0.85(Mg_{0.95}Ni_{0.05})TiO_3-0.15Ca_{0.6}La_{0.8/3}TiO_3$	1325 °C/4 h	24.61	102,000	−3.6	[15]
$(Mg_{0.6}Zn_{0.4})_{0.95}Ni_{0.05}TiO_3$	1200 °C/4h	19.30	165,000	−65.4	[16]
$0.88(Mg_{0.6}Zn_{0.4})_{0.95}Ni_{0.05}TiO_3-0.12Ca_{0.6}La_{0.8/3}TiO_3$	1225 °C/4 h	24.70	106,000	3.8	This work

3. Experimental Procedure

Traditional solid-state ceramic methods were utilized to synthesize samples of $(Mg_{0.6}Zn_{0.4})_{0.95}Ni_{0.05}TiO_3$, $Ca_{0.6}La_{0.8/3}TiO_3$, and $Ca_{0.8}Sm_{0.4/3}TiO_3$ from high-purity oxide powders (>99.9%): MgO, NiO, ZnO, $CaCO_3$, La_2O_3, Sm_2O_3, and TiO_2. First, the starting materials were mixed according to the stoichiometry: $(Mg_{0.6}Zn_{0.4})_{0.95}Ni_{0.05}TiO_3$, $Ca_{0.6}La_{0.8/3}TiO_3$, and $Ca_{0.8}Sm_{0.4/3}TiO_3$. Then, they were ground in distilled water for 24 h in a ball mill with agate balls. The mixed solution was dried in the oven and calcined at 1100 °C/4 h for $(Mg_{0.6}Zn_{0.4})_{0.95}Ni_{0.05}TiO_3$, 1100 °C/4 h for $Ca_{0.6}La_{0.8/3}TiO_3$, and 1250 °C/3 h for $Ca_{0.8}Sm_{0.4/3}TiO_3$ in a high-temperature furnace. The calcined reagents were mixed in the second step according to the formula of $x(Mg_{0.6}Zn_{0.4})_{0.95}Ni_{0.05}TiO_3$-$xCa_{0.6}La_{0.8/3}TiO_3/Ca_{0.8}Sm_{0.4/3}TiO_3$ and ground into a fine powder for 24 h. A 3.5 wt% of a 12% PVA solution as a binder (Polyvinyl alcohol 500, Showa) was added into the calcined powder, granulated by sieving through a 100 mesh, and pressed into pellets, 1.1 cm in diameter and 0.5 cm in thickness, under 200 MPa pressure. The pellets were sintered at temperatures ranging from 1175 °C to 1275 °C for 4 h in air. The heating and cooling rates of the high-temperature furnace were set at 10 °C/min to obtain high-quality samples.

The crystallization of the sintered bulks was checked by XRD using CuKα (λ = 0.15406 nm) with a Siemens D5000 diffractometer in the 2θ range from 20° to 80°. The lattice constant was calculated using software with the Rietveld method to fit the XRD patterns. [16] A.C. Larson, R.B. Von Dreele, Los Alamos Laboratory Report LAUR 86-748, Los Alamos National Laboratory, Los Alamos, NM, 1988. The microstructural observation of the sintered surface morphology was carried out using scanning electron microscopy equipped with energy-dispersive X-ray spectroscopy (EDS) and backscattered electronic image (BEI). The apparent densities of the sintered samples were measured using the Archimedes method. The ε_r and *Qf* were measured using the Hakki–Coleman dielectric resonator methodology [27], as improved by Courtney [28]. This method utilizes parallel conducting plates and coaxial probes in TE_{011} mode. TE represented transverse electric waves. The first two subscript integers denote the waveguide mode, and the third integer subscript indicates the order of resonance in an increasing set of discrete resonant lengths. The measurement system was connected to an vector network analyzer with Anritsu's model MS46122B (Atsugi, Japan). The τ_f value was measured with an identical setup but in the thermostat ranging from 20 °C to 80 °C. The following formula was utilized to obtain τ_f value (ppm/°C):

$$\tau_f = \frac{f_2 - f_1}{f_1(T_2 - T_1)} \tag{2}$$

where f_1 and f_2 represent the resonance frequencies at T_1 = 20 °C and T_2 = 80 °C, respectively.

4. Conclusions

In this study, $Ca_{0.6}La_{0.8/3}TiO_3$ and $Ca_{0.8}Sm_{0.4/3}TiO_3$-modified $(Mg_{0.6}Zn_{0.4})_{0.95}Ni_{0.05}TiO_3$ ceramics were investigated to obtain a near-zero temperature coefficient with appropriate dielectric properties. It showed mixed phases of $(Mg_{0.6}Zn_{0.4})_{0.95}Ni_{0.05}TiO_3$ and $Ca_{0.8}Sm_{0.4/3}TiO_3$ or $Ca_{0.6}La_{0.8/3}TiO_3$ accompanied by second phase $(Mg_{0.6}Zn_{0.4})_{0.95}Ni_{0.05}Ti_2O_5$. The permittivity and temperature coefficient values of $x(Mg_{0.6}Zn_{0.4})_{0.95}Ni_{0.05}TiO_3$-$(1 - x)$ $Ca_{0.8}Sm_{0.4/3}$ $TiO_3/Ca_{0.6}La_{0.8/3}TiO_3$ ceramics were controllable by adjusting the x value and the *Qf* value increase as the x value rose. It is worth noting that optimized $0.88(Mg_{0.6}Zn_{0.4})_{0.95}Ni_{0.05}TiO_3$–$0.12Ca_{0.6}La_{0.8/3}TiO_3$ ceramic systems possessed good microwave dielectric properties—a permittivity (ε_r) of 24.7, a *Qf* value of 106,000 GHz, and a τ_f value of 3.8 ppm/°C at 1225 °C/4 h—and so the system was considered an excellent candidate to fabricate substrates for wireless component applications in the future.

Author Contributions: Conceptualization, C.-L.P.; methodology, S.-H.L.; validation, C.-H.S.; formal analysis, C.-L.P.; investigation, S.-H.L.; data curation, Q.-Z.L.; writing—original draft preparation, C.-H.S. and S.-H.L.; writing—review and editing, S.-H.L.; visualization, S.-H.L.; supervision, S.-H.L.; project administration, S.-H.L.; funding acquisition, S.-H.L. All authors have read and agreed to the published version of the manuscript.

Data Availability Statement: The data are contained within the article.

Conflicts of Interest: The authors declare no conflict of interest.

Sample Availability: Samples of the compounds are not available from the authors.

References

1. Nakagoshi, Y.; Sato, J.; Morimoto, M.; Suzuki, Y. Near-zero volume-shrinkage in reactive sintering of porous $MgTi_2O_5$ with pseudobrookite-type structure. *Ceram. Int.* **2016**, *42*, 9139–9144. [CrossRef]
2. Lin, S.H.; Chen, Y.B. Crystal structure and microwave dielectric properties of $[(Mg_{0.6}Zn_{0.4})_{0.95}Co_{0.05}]_2TiO_4$ modified $Ca_{0.8}Sm_{0.4/3}TiO_3$ ceramics. *Ceram. Int.* **2017**, *43*, 296–300. [CrossRef]
3. Aljaafari, A.; Sedky, A. Influence of Fine Crystal Percentage on the Electrical Properties of ZnO Ceramic-Based Varistors. *Crystals* **2020**, *10*, 681. [CrossRef]
4. Bor, B.; Heilmann, L.; Domènech, B.; Kampferbeck, M.; Vossmeyer, T.; Weller, H.; Schneider, G.A.; Giuntini, D. Mapping the Mechanical Properties of Hierarchical Supercrystalline Ceramic-Organic Nanocomposites. *Molecules* **2020**, *25*, 4790. [CrossRef]
5. Palmero, P. Structural Ceramic Nanocomposites: A Review of Properties and Powders' Synthesis Methods. *Nanomaterials* **2015**, *5*, 656–696. [CrossRef] [PubMed]
6. Lin, S.H.; Chen, Y.B. Structure and characterization of B_2O_3 modified $yNd(Mg_{1/2}Ti_{1/2})O_3$-$(1-y)Ca_{0.8}Sr_{0.2}TiO_3$ ceramics with a near-zero temperature coefficient at microwave frequency. *Ceram. Int.* **2017**, *43*, 2368–2371. [CrossRef]
7. Freitas, A.E.; Manhabosco, T.M.; Batista, R.J.C.; Segundo, A.K.R.; Araújo, H.X.; Araújo, F.G.S.; Costa, A.R. Development and Characterization of Titanium Dioxide Ceramic Substrates with High Dielectric Permittivities. *Materials* **2020**, *13*, 386. [CrossRef] [PubMed]
8. Itaalit, B.; Mouyane, M.; Bernard, J.; Womes, M.; Houivet, D. Effect of Post-Annealing on the Microstructure and Microwave Dielectric Properties of $Ba(Co_{0.7}Zn_{0.3})_{1/3}Nb_{2/3}O_3$ Ceramics. *Appl. Sci.* **2016**, *6*, 2. [CrossRef]
9. Lin, S.H.; Lin, Z.Q.; Chen, C.W. Microwave dielectric characterization of $Ca_{0.6}(La_{1-x}Y_x)_{0.2667}TiO_3$ perovskite ceramics with high positive temperature coefficient. *Ceram. Int.* **2021**, *47*, 16828–16832. [CrossRef]
10. Tang, B.; Xiang, Q.; Fang, Z.; Zhang, X.; Xiong, Z.; Lid, H.; Yuan, C.; Zhang, S. Influence of Cr^{3+} substitution for Mg^{2+} on the crystal structure and microwave dielectric properties of $CaMg_{1-x}Cr_{2x/3}Si_2O_6$ ceramics. *Ceram. Int.* **2019**, *45*, 11484–11490. [CrossRef]
11. Sohn, J.H.; Inaguma, Y.; Yoon, S.O. Microwave Dielectric Characteristics of Ilmenite-Type Titanates with High Q Values. *Jpn. J. Appl. Phys.* **1994**, *33*, 5466. [CrossRef]
12. Huang, C.L.; Pan, C.L. Dielectric properties of $(1-x)$ $(Mg_{0.95}Co_{0.05})$ TiO_3–$xCaTiO_3$ ceramic system at microwave frequency. *Mater. Res. Bull.* **2002**, *37*, 2483–2490. [CrossRef]

13. Shen, C.H.; Pan, C.L.; Lin, S.H. A Study of the Effect of Sintering Conditions of $Mg_{0.95}Ni_{0.05}Ti_3$ on Its Physical and Dielectric Properties. *Molecules* **2020**, *25*, 5988. [CrossRef] [PubMed]

14. Wakino, K. Wakino. Recent developments of dielectric resonator materials and filters. *Ferroelectrics* **1989**, *91*, 69–86. [CrossRef]

15. Shen, C.H.; Huang, C.L. Microwave Dielectric Characteristics of $(Mg_{0.95}Ni_{0.05})$ TiO_3-$Ca_{0.8}Sm_{0.4/3}TiO_3$ Ceramic System. *J. Alloys Compd.* **2009**, *477*, 720–725. [CrossRef]

16. Shen, C.H.; Huang, C.L.; Shih, C.F.; Huang, C.M. A novel temperature-compensated microwave dielectric $(1-x)$ $(Mg_{0.95}Ni_{0.05})$ TiO_3-$xCa_{0.6}La_{0.8/3}TiO_3$ ceramics system. *Int. J. Appl. Ceram.* **2009**, *6*, 562–570. [CrossRef]

17. Shen, C.H.; Pan, C.L.; Lin, S.H.; Ho, C.C. Microwave Performance, Microstructure, and Crystallization of $(Mg_{0.6}Zn_{0.4})_{1-y}Ni_yTiO_3$ Ilmenite Ceramics. *Appl. Sci.* **2021**, *11*, 2952. [CrossRef]

18. Chen, Y.-B. The dielectric properties of $0.85MgTiO_3$–$0.15Ca_{0.6}La_{0.8/3}TiO_3$ with ZnO additions for microwave applications. *J. Alloys Compd.* **2009**, *477*, 883–887. [CrossRef]

19. Zhai, S.; Liu, P.; Fu, Z. Microwave dielectric properties of low-fired $[Mg0.98(Li0.5Bi0.5)0.02]2SiO4$–$Ca0.8Sm0.4/3TiO3$ composite ceramics. *J. Mater. Sci. Mater. Electron.* **2018**, *29*, 1298–1303. [CrossRef]

20. Liao, J.; Senna, M. Crystallization of titania and magnesium titanate from mechanically activated $Mg(OH)_2$ and TiO_2 gel mixture Mater. *Res. Bull.* **1995**, *30*, 385. [CrossRef]

21. Huang, C.L.; Pan, C.L. Low Temperature Sintering and Microwave Dielectric Properties of $(1-x)$ $MgTiO_3$-$xCaTiO_3$ Ceramics Using Bismuth Additions. *Jpn. J. Appl. Phys.* **2002**, *41*, 707. [CrossRef]

22. Shen, C.H.; Huang, C.L.J. Phase Evolution and Dielectric Properties of $(Mg_{0.95}M_{0.05}{}^{2+})$ Ti_2O_5 $(M^{2+}=Co, Ni, and Zn)$ Ceramics at Microwave Frequencies. *Am. Ceram.* **2009**, *92*, 384–388.

23. Gurevich, V.L.; Tagantsev, A.K. Intrinsic dielectric loss in crystals. *Adv. Phys.* **1991**, *40*, 719. [CrossRef]

24. Kim, E.S.; Yoon, K.H. Effect of nickel on microwave dielectric properties of $Ba(Mg_{1/3}Ta_{2/3})O_3$. *J. Mater. Sci.* **1994**, *29*, 830. [CrossRef]

25. Kim, I.T.; Kim, Y.; Chung, S.J. Order-disorder transition and microwave dielectric properties of $Ba(Ni_{1/3}Nb_{2/3})O_3$ ceramics. *Jpn. J. Appl. Phys.* **1995**, *34*, 4096. [CrossRef]

26. Penn, S.J.; Alford, N.M.; Templeton, A.; Wang, X.; Xu, M.; Reece, M.; Schrapel, K. Effect of porosity and grain size on the microwave dielectric properties of sintered alumina. *J. Am. Ceram.* **1997**, *80*, 1885–1888. [CrossRef]

27. Courtney, W.E. Analysis and Evaluation of a Method of Measuring the Complex Permittivity and Permeability Microwave Insulators. *IEEE Trans. Microwave Theory Tech.* **1970**, *18*, 476–485. [CrossRef]

28. Shannon, R.D.; Prewitt, C.D. Effective ionic radii in oxides and fluorides. *Acta Crystallogr.* **1969**, *25*, 925–946. [CrossRef]